Study by DNS of the effects of a shear thickening law on the Taylor-Couette flow

SYLVAIN GUILLOU AND RACHID MAKHLOUFI

Laboratoire Universitaire des Sciences Appliquées de Cherbourg, EA 4253, Université de Caen, Site Universitaire de Cherbourg, BP 78, 50130 Octeville, France, E-mail : sylvain.guillou@unicaen.fr

Résumé :

Etude de l'effet d'une loi rhéoépaississante sur les instabilités de Taylor-Couette par DNS.

L'impact d'une loi rhéologique munie d'un rhéo-épaississement local caractéristique de certains fluides réducteurs de traînée est étudié par DNS. Comparées au cas Newtonien, les expériences de DNS pour ce fluide (rhéo-fluidifiant avec un rhéo-épaississement local) montre des différences dans la transition de l'écoulement tourbillonnaire de Taylor (TVF) vers l'écoulement complètement turbulent (FTF) : les écoulements tourbillonnaires ondulaires et modulés sont inhibés et remplacés par un écoulement de Taylor (TVF) perturbé. Le nombre de cellules est réduit.

Abstract:

The pattern formation and stability of a drag reducing fluid in a Taylor-Couette geometry is studied here by Direct Numerical Simulation. When compared to the Newtonian case, DNS experiments performed on this fluid (shear-thinning with a local shear thickening) show differences in the transition from the Taylor Vortex Flow to the Fully Turbulent Flow : the Wavy Vortex Flow and Modulated Vortices Flow are inhibited and replaced by a disturbed TVF and the Turbulent Taylor Vortex flow presents only two non-circular cells. Furthermore, the larger values of R_{ef} for the drag-reducing fluid, compared to the values of Re in the Newtonian fluid, indicate a delay in the appearance of the turbulence.

Key Words: Drag reduction, Taylor-Couette flow, Direct Numerical Simulation, Turbulence

1 Introduction

Drag reduction is a physical phenomenon characterised by a significant reduction of friction under turbulent flow. Since its discovery, more than half a century ago, and despite the numerous works on this subject (Zakin et al.[1] and references therein), the origin of this phenomenon is not fully clarified.

In the case of an aqueous solvent, for example, the presence of a small amount of a polymer or a surfactant in the solvent modifies the fluid structure and thus its initial rheology. The behaviour of the resulting fluid (drag-reducing) leads to a significant reduction of the wall-friction by changing the turbulence flow structures.

One way to contribute to the understanding of this phenomenon is to consider the rheology of the drag-reducing fluid and its impact on the turbulent flow structure. Numerically, many authors have run DNS experiments. One can quote the works of Orlandi [2], Den Toonder et al. [3,4], Manhart [5], Sureshkumar et al. [6], Dimitropoulos et al. [7], De Angelis et al. [8], Housiadas and Beris [9], Yu et al. [10], Guillou and Makhloufi [11], or Rudman et al. [12]. However, all these studies were performed in a circular pipe or plan channel geometries.

The aim of this work is to study the impact of a drag reducing fluid (Fig. 1) on the Taylor-Couette instabilities in the transition region between laminar and turbulent flows. The rheology of this fluid is characterised by a general shear-thinning behaviour with a significant local shear-thickening.

2 Problem description

The flow is confined, here, between two concentric cylinders (Fig. 2). The inner cylinder (of radius R_1) is rotated (at the velocity Ω_1) and the outer cylinder is stationary (of radius R_2). For this study, the numerical model (SUDRES3D for Surfactant Drag Reduction Study) developed by Guillou and Makhloufi [11] to

study the friction coefficient in a fully turbulent plane channel flow, was rewritten in cylindrical coordinate system. Following Guillou and Makhloufi [11], the viscous behaviour observed on Fig. 1 can be modelled by eqs. 1, by a combination of two Carreau behaviours given by eqs. (2). μ_∞ and μ_0 are respectively the viscosity for infinite and zero shear rate, n gives the slope of the viscosity curve in the power law region whereas λ represents the reciprocal shear rate of the transition between the first Newtonian plateau and the power law region. $\dot{\gamma}_c$ is the critical shear rate which corresponds to the passage from one behaviour to the other, whereas γ_0 is the range of $\dot{\gamma}_c$ where the solution is a linear combination of the two behaviours.

$$\mu(\dot{\gamma}) = \frac{\mu_1(\dot{\gamma}) + \mu_2(\dot{\gamma})}{2} + \frac{\mu_1(\dot{\gamma}) - \mu_2(\dot{\gamma})}{2} \tanh\left(\frac{\dot{\gamma} - \dot{\gamma}_c}{\gamma_0}\right) \quad (1)$$

$$\mu_i(\dot{\gamma}) = \mu_{\infty_i} + \left(\mu_{0_i} - \mu_{\infty_i}\right)\left(1 + \left(\lambda_i \dot{\gamma}\right)^2\right)^{(n_i - 1)/2} \quad (2)$$

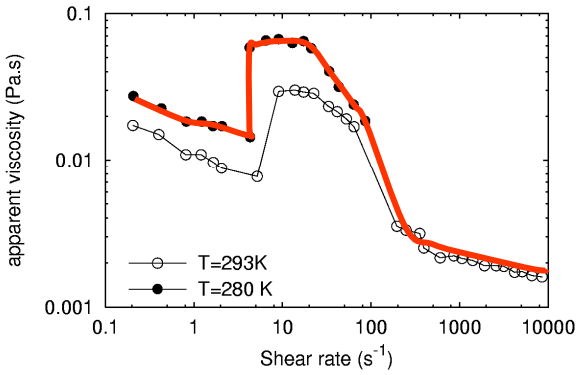

FIG. 1. Apparent viscosity of Ethoquad O/12 (500ppm) + NaSal (330 ppm) aqueous solution. Experimental data (Usui et al. [13]) and viscous models for T=280K (Table 1).

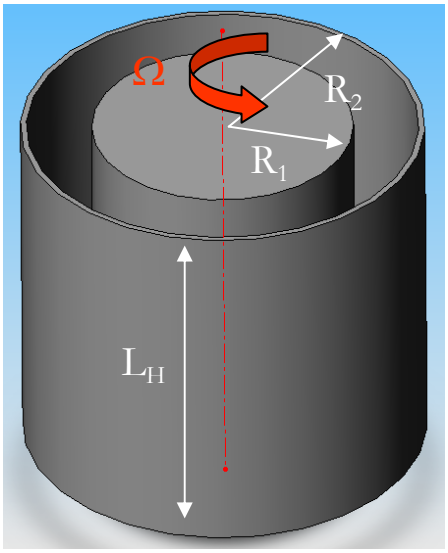

FIG. 2. Configuration diagram: R_1 and R_2 are the radius of the inner and the outer cylinder, and L_H is the height of the cylinders (here $R_1=R_2*2/3$, $L_H=6.28*(R_2-R_1)/2$).

3 Mathematical background

The basic equations describing this incompressible flow are as follows:

$$\begin{cases} \nabla \cdot \mathbf{u} = 0 \\ \dfrac{d\mathbf{u}}{dt} = -\dfrac{1}{\rho}\nabla p + \dfrac{1}{\rho}\nabla \cdot \boldsymbol{\tau} \end{cases} \quad (3)$$

Where **u**, ρ, p and **τ** are respectively the velocity vector, the density, the pressure and the deviatoric stress tensor. d/dt denotes the material derivative, and ∇ denotes the gradient operator. The behaviour of the fluid is taken into account by the modelling of the deviatoric stress tensor.

$$\boldsymbol{\tau} = 2\mu(II_{2D})\mathbf{D} \quad (4)$$

The viscous generalised flow type is adopted here. It leads to the generalised Newtonian constitutive equation (8), where $\mathbf{D}=1/2(\nabla\mathbf{u}+{}^t\nabla\mathbf{u})$ is the rate-of-strain tensor, and μ is the dynamic viscosity of the solution, which depends on the second invariant of the rate-of-strain tensor II_{2D}. For an incompressible fluid, this parameter is given by $II_{2D}= -2\mathbf{D}:\mathbf{D}$. In the case of a simple shear flow, $\sqrt{|II_{2D}|}$ is equal to shear rate $\dot{\gamma}$.

The reference parameters are the gap half-width h=(R_2-R_1)/2, the fluid density ρ, the solvent viscosity μ_s, and the velocity at the inner cylinder $\Omega_1 R_1$. A first Reynolds Number based on the viscosity of the solvent is written (5), and then another one is based on the viscosity of the solution at the inner cylinder μ_{fw} (6). Finally, the equations (eqs. 3) become (eqs. 7). The Taylor number (rate between the centrifugal force and the viscous drag force) is defined by the relation (8).

$$R_e = \frac{\Omega R_1 (R_2 - R_1)}{\nu_s} \tag{5}$$

$$R_{ef} = \frac{\Omega R_1 (R_2 - R_1)}{\nu_{fw}} \tag{6}$$

$$\begin{cases} \nabla^* \cdot \mathbf{u}^* = 0 \\ \dfrac{d\mathbf{u}^*}{dt^*} = -\nabla^* p^* + \dfrac{2}{R_e} \nabla^* \cdot \boldsymbol{\tau}^* \end{cases} \tag{7}$$

$$T_a = \frac{\Omega^2}{\nu^2} \frac{R_2 + R_1}{2} (R_2 - R_1)^2 = R_e^{\,2} \frac{R_2^{\,2} - R_1^{\,2}}{2 R_1^{\,2}} \tag{8}$$

A Finite Difference Method on a staggered grid and a fractional-step method (projection technique) are used to solve the three-dimensional equations. The time dicretisations used are respectively a second-order-explicit-Adams-Bashforth scheme and a Cranck-Nicholson scheme to account for the convective and diffusive terms in the momentum equation. The time step is calculated in order to respect the Courant-Friedrich-Levy's condition (CFL). The spatial differential operators are approximated by second-order central differences. The mesh is uniform in the tangential directions whereas non-uniform point distribution is used in the radial one. The flow is periodic in the tangential direction. The inner wall moves with the velocity Ω_1.

For the simulations the following non-dimensional sizes were used: R_1^*=4, R_2^*=6, L_H^*=6.28. The meshes used are 41*161*81 or 61*161*81 in the direction $\mathbf{e}_r$, $\mathbf{e}_\theta$ and $\mathbf{e}_z$. Periodical conditions are used in polar- and z-directions, whereas no-slip conditions are used at the walls. Analytical solution of the Couette flow is used as initial condition. Simulations are realized for a simple Newtonian fluid and for the shear-thickening fluid of fig. 1. For the latter, the parameters of the table 1 are used and the size of the gap is fixed at 26 mm.

Table 1: Parameters of the combined law used to fit the viscous behaviour (Ethoquad O/12) of fig. 1 at T=280K, with $\dot{\gamma}_c = 4.29 s^{-1}$ and $\gamma_0 = 0.25 s^{-1}$.

μ (Pa.s)	μ_0 (10^{-3}Pa.s)	μ_∞ (10^{-3}Pa.s)	λ (s)	n
μ1	66	3	0,03	-0,5
μ2	28	3	1,8	0,55

4 Results

Fig. 3 and Fig. 5 represent the instantaneous velocity fields in a gap cross-section and the 3D-isosurface of instantaneous helicity for the Newtonian fluid and for several Reynolds numbers, whereas Fig.4 and Fig.6 show the same results for the drag-reducing fluid.

For the Newtonian fluid, two pairs of counter rotating cells are observed (Fig.3.a and Fig.5.a) in the transition from the Couette flow to the Taylor Vortex Flow (TVF). This is a four-cell primary flow. At higher Reynolds numbers, oscillations of the cores' position (axial- and z- positions) appear (Fig. 3.b and Fig.5.b), creating a waving evolution of the cell along the θ-direction: this is the Wavy Vortex Flow (WVF). For very large Reynolds numbers, the flow becomes more complicated, the waves are not regular (Fig.3.c and Fig.5.c): this corresponds to the Modulated Waves Flow (MVF). Then the flow becomes turbulent with the presence of four major stable cells (Fig.3.d and Fig.5.d) which correspond to the Turbulent Taylor Vortices (TTV). Finally, for very high Reynolds numbers, the flow becomes fully turbulent (Fig.3.e

and Fig.5.e) with eddies of different sizes. These results are in agreement with the literature on the Newtonian Taylor-Couette flow (Koschmieder et al. [14], DiPrima and Swinney [15]).

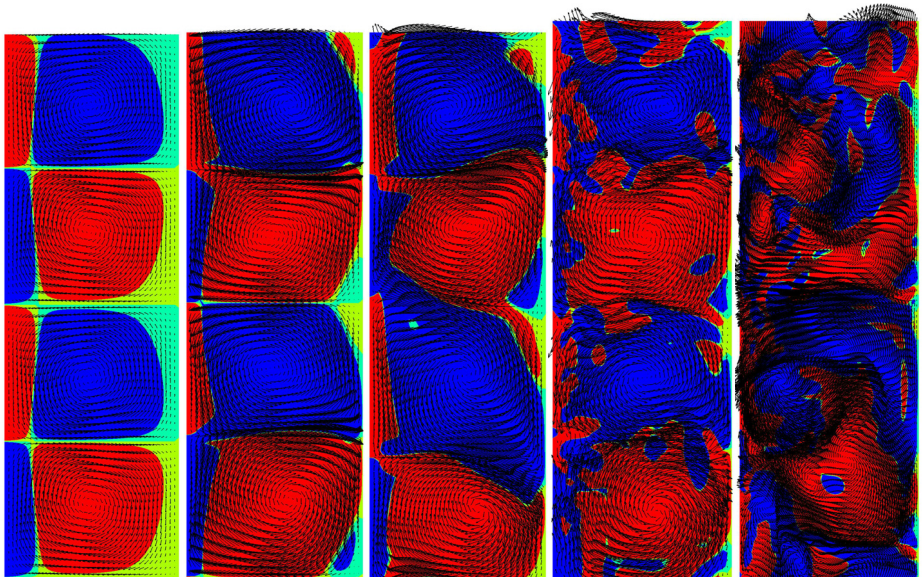

FIG.3. Velocity and helicity fields in a gap cross-section (positive and negative values representing the direction of the eddies) for the Newtonian fluid: a) R_e=100; b) R_e=1200; c) R_e=1600; d) R_e=4000; e) R_e=5200.

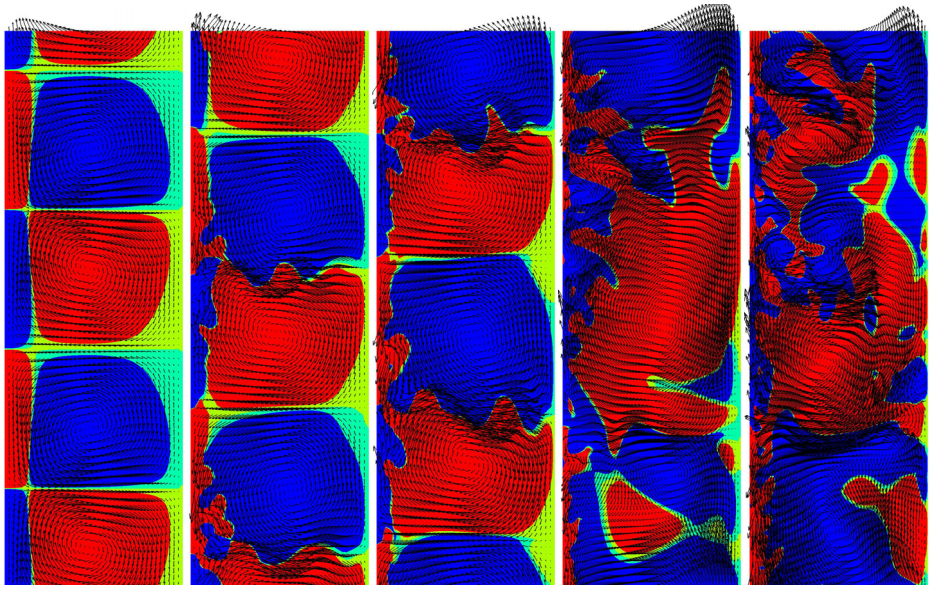

FIG.4. Velocity and helicity fields in a gap cross-section (positive and negative values representing the direction of the eddies) for the aqueous solution of Ethoquad: a) Ref=240; b) Ref=4434; c) Ref=6677; d) Ref=8056; e) Ref=12185.

Concerning the drag-reducing fluid, the description of the behaviour is made here using the Reynolds number based on the viscosity of the fluid at the wall (R_{ef}) rather than with the Reynolds number based on the viscosity of the solvent (R_e). However, the corresponding Reynolds number R_e is given between commas for information. For R_{ef}=66 (R_e=4000), the flow is of Couette type. For higher R_{ef}, we observe a Taylor Vortex Flow with four cells (Fig.4.a and Fig.6.a, R_{ef}=240, R_e=8000). This TVF is stable until R_{ef}=4434 (Re=20000) at which point instabilities appear between the coupled vortices (Fig4.b and Fig6.b) in the region close to the inner cylinder and the flow goes from the inner cylinder to the outer one. It seems that this instability is produced at the inner cylinder and transmitted by the Taylor Vortex motion towards the outer cylinder. This is confirmed by the results for Ref=6677 (Re=25000) for which the instabilities are greater and act along the cross direction (Fig.4.c and Fig.6.c). For Ref=8056 (Re=30000). The flow becomes turbulent with two major vortices. It can be compared to the turbulent TTV flow type. For R_{ef}=12185 (R_e=40000), the flow is fully turbulent.

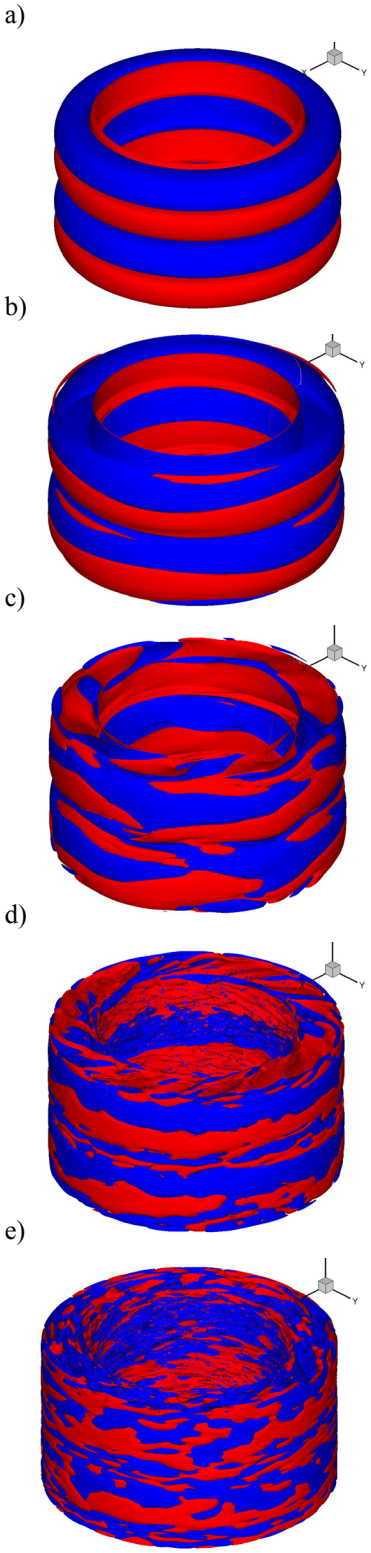

FIG. 5. Isosurfaces of the Helicity for the Newtonian fluid: a) Re=100; b) Re=1200; c) Re=1600; d) Re=4000; e) Re=5200. The positive (red) and negative (blue) values represent the direction of the eddies

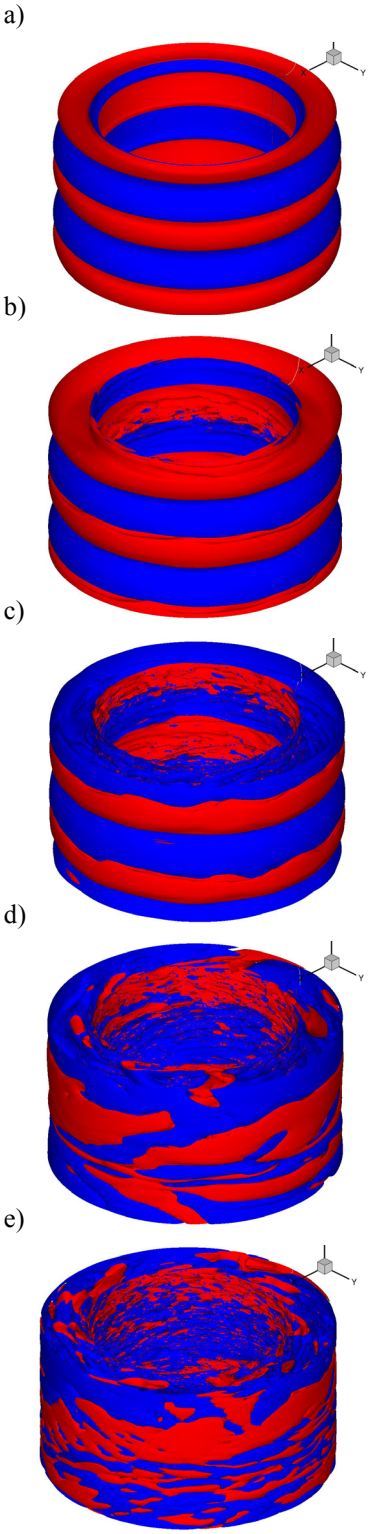

FIG. 6. Isosurfaces of the Helicity for the aqueous solution of Ethoquad: a) Ref=240; b) Ref=4434; c) Ref=6677; d) Ref=8056; e) Ref=12185. The positive (red) and negative (blue) values represent the direction of the eddies

The simulations for the Newtonian fluid show six types of flow: Couette Flow; Taylor Vortex Flow; Wavy Vortex Flow; Modulated waves Flow; Turbulent Taylor Vortices and Fully Turbulent Flow. The simulations for the drag-reducing fluid show only five flow types: Couette Flow; Taylor Vortex Flow; disturbed TVF; Two-cell Turbulent Taylor Vortices and Fully Turbulent Flow.

The Wavy Vortex Flow does not exist for the drag-reducing fluid, nor does than the MWF. They are replaced by a disturbed TVF which is not regular along the θ-direction and does not form regular waves. Moreover, they are only two non-regular TTVs (Fig.5.d). The great values of R_{ef} for the drag-reducing fluid in comparison of the values of R_e for the Newtonian fluid indicate that the new behavior induces a delay in the appearance of the turbulence.

5 Conclusion

A numerical model was developed to study in a Taylor-Couette geometry the flow structure of a Newtonian and a drag-reducing fluid having a general shear-thinning behaviour with local shear-thickening.

In such geometry, the transition sequence from the Couette flow to the TVF is similar for the two fluids. However, great differences appear for other transitions. For the drag-reducing fluid, there is no WVF, nor MVF, and the TTV flow presents only two non-circular cells.

Furthermore, the greater values of R_{ef} for the drag-reducing fluid in comparison to the values of R_e for the Newtonian fluid indicate that the drag behavior induces a delay in the appearance of the turbulence.

References

[1] Zakin J.L., Lu B. and Bewersdorff H.-W., Surfactant drag reduction, Reviews in Chemical Engineering, **14** (1998), 253-320.
[2] Orlandi P., A tentative approach to the direct simulation of drag reduction by polymers, *Journal of Non-Newtonian Fluid Mechanics*, **60** (1995) 277-301.
[3] Den Toonder J.M.J., Nieuwstadt F.T.M. and Kuiken G.D.C., The role of elongational viscosity in the mechanism of drag reduction by polymer additives, Applied Scientific Research, **54** (1995), 95-123.
[4] Den Toonder J.M.J., Hulsen M.A., Kuiken G.D.C and Nieuwstadt F.T.M., Drag reduction by polymer additives in a turbulent pipe flow: numerical and laboratory experiments, J. Fluid Mech., **327** (1997) 193-231.
[5] Manhart M., Rheology of suspensions of rigid-rod like particles in turbulent channel flow, Journal of Non-Newtonian Fluid Mechanics, **112** (2003) 269-293.
[6] Sureshkumar R., Beris R. and Handler R.A., Direct numerical simulation of turbulent channel flow of a polymer solution, Phys. Fluids, **9** (1997) 743-755.
[7] Dimitropoulos C.D., Sureshkumar R. and Beris N., Direct numerical simulation of viscoelastic turbulent channel flow exhibiting drag reduction: effect of the variation of rheological parameters, J. Non-Newtonian Fluid Mech., **79** (1998) 433-468.
[8] De Angelis E., Casciola C.M. and Piva R., DNS of wall turbulence: dilute polymers and self-sustaining mechanisms, Computers & Fluids, **31** (2002) 495-507.
[9] Housiadas K. D. and Beris A. N., An efficient fully implicit spectral scheme for DNS of turbulent viscoelastic channel flow, *J. of Non-Newtonian Fluid Mechanics*, **122** (2004) 243-262.
[10] Yu B. and Kawaguchi Y., Direct numerical simulation of viscoelastic drag-reducing flow: a faithful finite difference method, Journal of Non-Newtonian Fluid Mechanics, **116** (2004) 431-466.
[11] Guillou S. and Makhloufi R., Effect of a shear-thickening fluid on drag reduction studied by Direct Numerical Simulation, International Journal for Non-Newtonian Fluid Mechanics, **144** (2007) 73-86.
[12] Rudman M., Blackburn H.M., Graham L.J.W. and Pullum L., Turbulent pipe flow of shear-thinning fluids, J. of Non Newtonian Fluid Mechanics, **118** (2004) 33-48.
[13] Usui H., Itoh T. and Saeki T., On pipe diameter effects in surfactant drag-reducing pipe flows, Rheo. Acta, **37** (1998) 122-128.
[14] Koschmieder E.L., Bénard Cells and Taylor Vortices, Cambridge University Press, Cambridge, UK (1993).
[15] DiPrima RC and Swinney HL, Hydrodynamic Instabilities and the Transition to Turbulence, ed. HL Swinney and JP Gollub, Springer, Berlin (1981) chapter 6, pp139-80.